Phase-separation kinetics of a multicomponent alloy

S. Mazumder* and D. Sen
Condensed Matter Physics Division, Bhabha Atomic Research Centre, Trombay, Mumbai 400085, India

I. S. Batra, R. Tewari, G. K. Dey, and S. Banerjee
Materials Science Division, Bhabha Atomic Research Centre, Trombay, Mumbai 400085, India

A. Sequeira
Condensed Matter Physics Division, Bhabha Atomic Research Centre, Trombay, Mumbai 400085, India

H. Amenitsch
Institute for Biophysics and X-ray Structure Research, Austrian Academy of Science, Steyrerg. 17, 8010 Graz, Austria

S. Bernstorff
Sincrotrone Trieste, Area Science Park, I-34012 Basovizza, Trieste, Italy
(Received 12 August 1998; revised manuscript received 22 January 1999)

Phase separation kinetics of multicomponent 350-grade maraging steel has been investigated on both recrystallized as well as cold-worked specimens by small-angle x-ray scattering, wide angle x-ray scattering, and transmission electron microscopy at two different temperatures, viz. 430 °C and 510 °C, for different aging times. Unlike previous observations, at both the temperatures, dynamical scaling behavior is observed at the early stages of phase separation accompanied by diffuse interface of the secondary phases. Porod exponents have been found to be greater than 4. At late stages, the precipitate-matrix interface becomes sharp — the Porod exponent is close to 4 but clear deviation from the dynamical scaling behavior is evident. At 430 °C, the phase separation is attributed to the formation of an ordered ω phase through a mechanism involving chemical ordering and the ω-like lattice collapse in the bcc structure. Time (t) dependent population averaged precipitate radius follows $t^{1/5}$ power law indicating cluster diffusion mechanism of Binder-Stauffer type for the entire range, 30 min–72 h, of aging time. At 510 °C, the phase separation is attributed to the formation of Ni_3(Ti,Mo) with DO_{24} structure through the process of nucleation and growth. Average precipitate radius follows $t^{1/3}$ Lifshitz-Slyozov power law for the entire range, 5 min–18 h, of aging time. The system, despite being multicomponent and complex, appears to follow two distinct time-temperature-transformation curves. As far as the effect of cold work on phase-separation behavior is concerned, it has been found that cold work facilitates the growth of the precipitates. Also, it narrows down the size distribution and enforces strong spatial correlation of the precipitates. Cold working the material is found to be detrimental to the dynamical scaling behavior. [S0163-1829(99)06325-0]

I. INTRODUCTION

The kinetics of phase separation from a homogeneous phase into a two phase region is a subject of continuing fascination[1–18] for the last several decades. These studies are of immense practical significance for metallic alloys as the kinetics of phase separation and the microscopic structures of the secondary phases determine many properties of the alloys for their technological end use. In this regard, the dynamical scaling behavior during phase separation is of considerable importance towards understanding the phase separation of an alloy system. Scaling hypothesis, originally motivated by computer simulation results,[4,6] has been proved to be valid on a number of binary alloys.[5,7–10] For an alloy system, according to generalized scaling theories,[11–13,16] the time-dependent scattering function $S(q,t)$ in the scaling regime obeys simple scaling law $S(q,t) \sim L(t)^d F(qL(t))$ where q is the length of the wave vector, $L(t)$ is the time-dependent characteristic length and d is the dimensionality of the system. The scaling function $F(qL(t))$ in the domain of large q ($qL(t) \gg 1$) asymptotically approaches $F(x) \sim x^{-(d+n)}$ where n is the number of components in the vector order-parameter field exhibiting the scaling behavior. The aforementioned scaling law reduces to well-known Porod law $S(q,t) \sim q^{-4}$ for a three-dimensional system with single order parameter and sharp interfaces.

Experiments[5,7–10] on binary alloys show that the scaling phenomenon holds only at the late stages of phase separation when $S(q,t)$ exhibits q^{-4} dependence for high-q values. At the initial stage, the scaling law is not operative and $S(q,t)$ exhibits q^{-2} dependence for high-q values. The investigation of scaling phenomena in the case of liquid crystals with multicomponent order parameter indicated[14,15] the validity of the scaling hypothesis. But, to the best of our knowledge, similar investigation on multicomponent alloy systems is yet to be carried out. The present investigation on phase-separation behavior of 350-grade maraging steel, a material of strategic importance, is a step in this direction.

The current study shows that the dynamical scaling law holds, in contrast to its validity during late stages of phase

 ©1999 The American Physical Society

separation in binary alloys,[5,7–10], during the early stages of phase separation in the multicomponent alloy maraging steel. However, the scaling phenomenon is valid only at the early stage when the interface between the secondary phase and matrix is diffused. At the late stages the interface becomes sharp but the dynamical scaling law does not hold good.

Maraging steels, developed first[19] in the 1960s at the International Nickel Company and well known for their high strength-to-weight ratio, high toughness, and easy machinability in the solution annealed condition, are extensively used in strategic applications. As the name indicates, high strength in these steels is developed by precipitation hardening of the relatively soft martensitic matrix. Precipitation hardening of this alloy is therefore an important processing step to achieve the desired properties for a specific end use. The evolution of microstructure of the material with aging treatments has been extensively investigated,[20–23] primarily by TEM. These studies have helped in the identification of crystallography of the precipitating phases.

Servant and co-workers[24,25] employed the complementary techniques of small-angle x-ray scattering (SAXS) and transmission electron microscopy (TEM) for studying the phase separation behavior of a 300-grade maraging steel at aging temperatures of 458 °C and below and reported the formation of both disordered and chemically ordered ω phase. An attempt was also made to establish the growth of radius of gyration of the precipitates with aging time. It is noteworthy that the ordered ω is of current interest[26] as the mechanism of its formation involves a combination of displacive and replacive ordering. In the present study, we address the issue of the competition between the formation of ω-like structures through a combination of displacive and replacive ordering vis-à-vis precipitation of intermetallic phases through classical nucleation and growth.

The formation of the ω phase in a bcc lattice can be conceived as an introduction of a longitudinal displacement wave[27] in the lattice. In fact the athermal $\beta \rightarrow \omega$ transition has been shown to be a displacive transition. However, formation of ordered ω structures involve a combination of displacement wave and chemical ordering. At the early stages of precipitation, which has been investigated in the present work, the development and amplification of displacement and concentration waves leads to the formation of ordered ω structures. During the evolutionary stages such inhomogeneities are expected to have diffuse interfaces as far as the composition is concerned.

We also investigate the effect of cold rolling on the precipitation phenomena. It is well known that cold working an alloy increases the density of dislocations in it. These dislocations may provide paths for diffusion of solute atoms for the growth of precipitates as well as sites for nucleation of precipitates under appropriate conditions of aging. In maraging steels of 18 wt % Ni variety, a high density of dislocations is introduced due to the lattice invariant deformation associated with the transformation of austenite to martensite during cooling. These transformation related crystallographically necessary dislocations are known to strengthen the martensite. Cold deformation of martensite increases the dislocation density further, albeit only marginally. This is inferred from the low work hardening rates seen in these steels at ambient deformation temperatures.

A study of the response of the cold-worked martensite to aging treatments is considered necessary since, quite often, components are aged without prior recrystallization treatments. The study becomes even more important in view of the fact that, at temperatures around 450 °C, ω related phases are known to form in 18 wt % Ni steels.[25] The formation of ω through lattice collapse mechanism takes place at a large number of sites (approximately 10^{19} sites per cm^3) in the matrix and cold work can influence this density.

II. EXPERIMENT

Two specific temperatures, viz. 430 °C and 510 °C, have been suitably chosen in order to study the competition between the formation of the ordered ω phase and the intermetallic precipitates, the former known to occur at lower temperatures. The selection of higher aging temperature has also been governed by the fact that the chosen steel (composition 18 wt % Ni, 4.2 wt % Mo, 12.5 wt % Co, 1.7 wt% Ti, 0.1 wt % Al, 0.02 wt % Mn, 0.004 wt % C, and rest Fe) is conventionally hardened by vacuum aging at 510 °C. At each temperature, the specimens have been aged for different durations of time. At 510 °C, the aging time ranges from 5 min–18 h while at 430 °C, time ranges between 30 min and 72 h.

Simultaneous small-angle x-ray scattering (SAXS) and wide-angle scattering (WAX) measurements have been carried out at synchrotron source, ELETTRA, Trieste, Italy using 16 keV (wavelength $\lambda = 0.077$ nm) branch of SAXS beamline.[28] Scattering functions have been estimated after subtracting the suitably normalized scattering functions of the recrystallized specimens from the corresponding normalized scattering functions for the aged specimens. The normalization of the scattering functions have been carried out for unit thickness of the sample. Thickness of each specimen has been calculated from the transmission of the specimen and linear absorption coefficient (309.012 cm^{-1}) of this material.

III. DATA INTERPRETATION AND DISCUSSION

Figures 1and 2 show the time-dependent scattering function $S(q,t)$ [$q = 4\pi \sin(\theta)/\lambda$, where 2θ is the scattering angle] at 430 and 510 °C, respectively. As evident from Figs. 1 and 2, with increasing aging time the scattering function becomes sharp with the position of the maxima shifting towards smaller wave vectors and with the peak intensity increasing quite sharply. These observations indicate that both growth and the spatial correlation of the secondary phase intensify with aging. Figure 3 shows the effect of cold rolling on precipitation phenomena as manifested on the scattering function. Here also the scattering functions have been obtained after subtracting the suitably normalized scattering functions of the cold rolled and nonaged specimens from the corresponding ones for the cold-worked and aged specimens. From Fig. 3 it is evident that cold work facilitates the growth of the precipitates and their spatial correlation.

Porod exponents, as estimated from ln(intensity) vs ln(q), in the q range 1.8–2.86 nm^{-1} for various specimens are

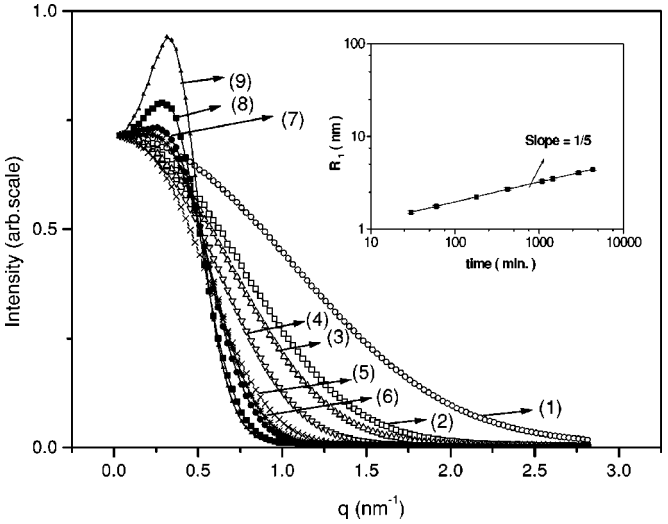

FIG. 1. Time evolution of the scattering function $S(q,t)$ of 350-grade maraging steel aged at 430 °C for different durations of time as mentioned below against each profile. (1) recrystallized, (2) 30 min, (3) 1.0 h, (4) 3.0 h, (5) 7.0 h, (6) 18.0 h, (7) 24.0 h, (8) 48.5 h, (9) 72.0 h. The inset shows the time evolution of average precipitate radius showing $t^{1/5}$ law.

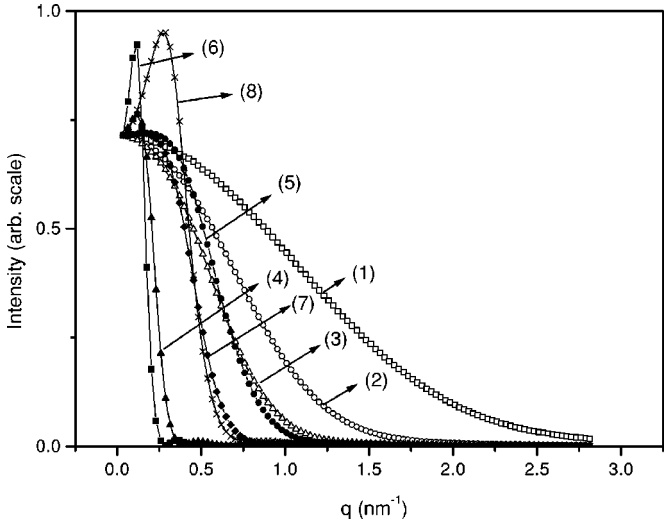

FIG. 3. Scattering function $S(q,t)$ of cold-rolled and recrystallized specimen of 350-grade maraging steel for some aging conditions as mentioned below. (1) recrystallized (RC); (2) cold rolled (CR); (3) RC, 430 °C and 7.0 h; (4) CR, 430 °C and 7.0 h; (5) RC, 430 °C and 18.0 h; (6) CR, 430 °C and 18.0 h; (7) RC, 510 °C and 1.0 h; (8) CR, 510 °C and 1.0 h.

listed in Table I. The deviation of the Porod exponents from 4 is more pronounced for specimens aged at 430 °C. The proximity of the values to 4 for specimens aged for long time are indicative of well defined interface. The positive deviation of the Porod exponents of the profiles from 4 is indicative of the diffuse interface between the precipitates and the matrix which arises essentially due to the presence of composition modulation in the matrix. This is expected as the formation of both the ordered ω and $Ni_3(Ti,Mo)$ phases involve development and amplification of concentration waves of appropriate wavelength in the prenucleation stage. While in the former case a displacement wave interferes with the concentration wave in the bcc lattice, the latter involves a structural transition into the fcc lattice and a growth of a concentration wave therein.

This conjecture is also supported by a model calculation[29] of scattering profile from a spherically symmetric inhomoge-

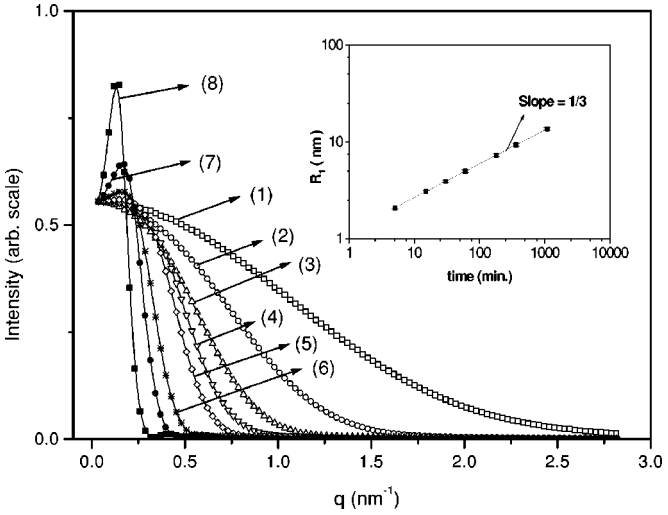

FIG. 2. Time evolution of the scattering function $S(q,t)$ of 350-grade maraging steel aged at 510 °C for different durations of time as mentioned below against each profile. (1) recrystallized, (2) 5 min, (3) 15 min, (4) 30 min, (5) 1.0 h, (6) 3.0 h, (7) 6.0 h, (8) 18.0 h. The inset shows the time evolution of average precipitate radius showing $t^{1/3}$ law.

TABLE I. Porod exponents of the specimens.

Sample specification (aging temperature and time)	Porod exponent
Recrystallized (RC)	5.23±0.12
RC, 430 °C and 30 min	5.12±0.13
RC, 430 °C and 1.0 h	5.09±0.13
RC, 430 °C and 3.0 h	4.89±0.12
RC, 430 °C and 7.0 h	4.78±0.13
RC, 430 °C and 18.0 h	4.56±0.14
RC, 430 °C and 24 h	4.25±0.15
RC, 430 °C and 48.5 h	4.10±0.12
RC, 430 °C and 72.0 h	4.003±0.12
RC, 510 °C and 5 min	4.75±0.16
RC, 510 °C and 15 min	4.54±0.14
RC, 510 °C and 30 min	4.343±0.132
RC, 510 °C and 1.0 h	4.12±0.12
RC, 510 °C and 3.0 h	3.998±0.11
RC, 510 °C and 6.0 h	4.001±0.11
RC, 510 °C and 18.0 h	4.015±0.11
Cold rolled (CR)	4.098±0.107
CR, 430 °C and 7.0 h	4.012±0.16
CR, 430 °C and 18.0 h	4.024±0.11
CR, 510 °C and 1.0 h	4.035±0.11

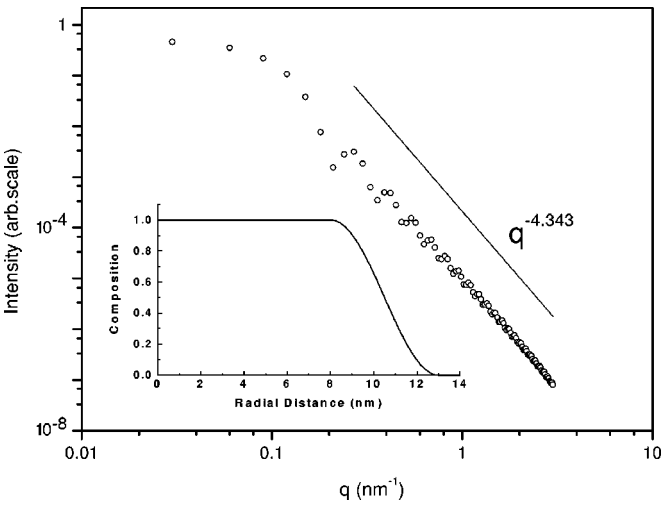

FIG. 4. The scattering profile of a polydisperse model system where the interface composition has a gradual variation as shown by a schematic figure given in the inset. At large q, the profile follows a power law $\sim q^{-4.343(0.14)}$. The solid line is only a guide to the eye.

neity with diffuse interface as shown by the inset of Fig. 4. The composition has been assumed to have sinusoidal variation at the interface. Polydispersity following square-wave size distribution has been introduced to smoothen the profile, shown in Fig. 4, represented in form of ln(intensity) vs ln(q). The Porod exponent of the calculated profile has been found to be 4.343 ± 0.14. Porod exponent can be raised as high as 8 by increasing the width[30] of the diffused interface.

The observation of diffuse interface is a demonstration of the unique capability of the small-angle scattering technique

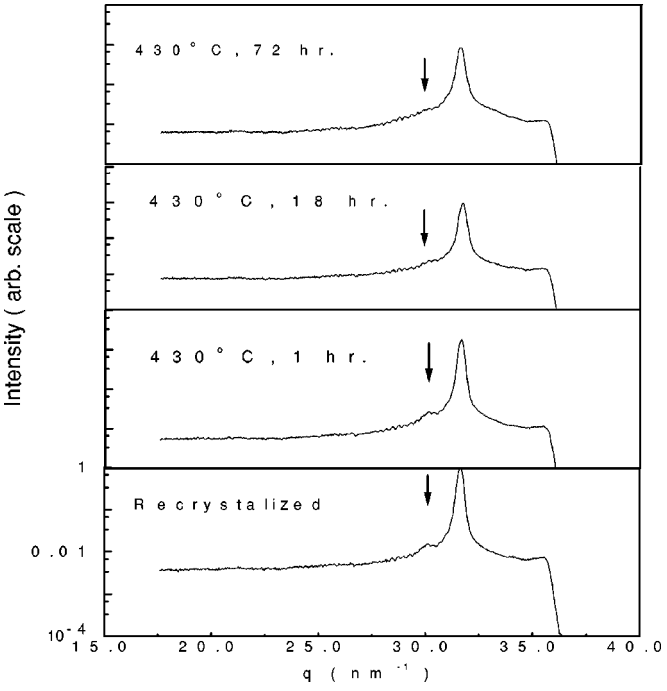

FIG. 5. WAXS profiles of specimens aged at 430 °C for some specified duration of time. The side peak is indicated by the arrow. The strong peak is due to reflection from (110) of the martensite bcc matrix.

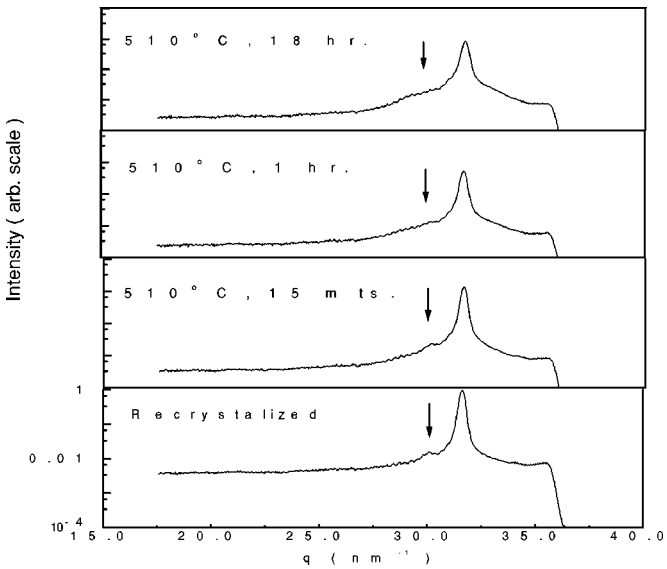

FIG. 6. WAXS profiles of specimens aged at 510 °C for some specified duration of time. The side peak is indicated by the arrow.

over other complementary techniques like TEM. The concentration modulation gives rise to the side peak observed in the WAXS profiles, as shown in Figs. 5 and 6, with a characteristic wavelength (~ 0.21 nm) in the system and can also explain the diffuse interface of the precipitates. With aging this modulation dies down. At 510 °C, this modulation

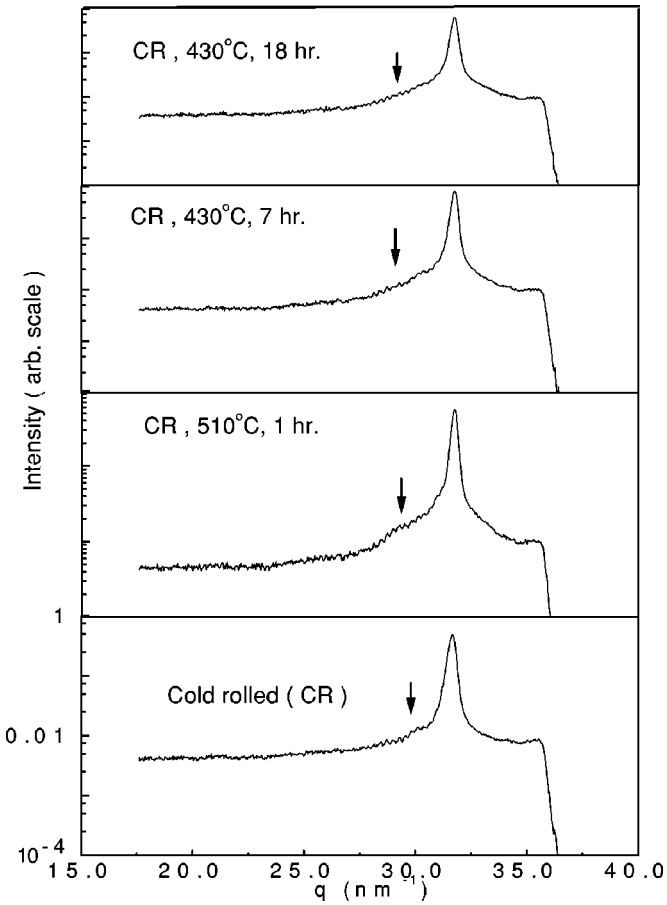

FIG. 7. WAXS profiles of cold-rolled specimens. The side peak is weak.

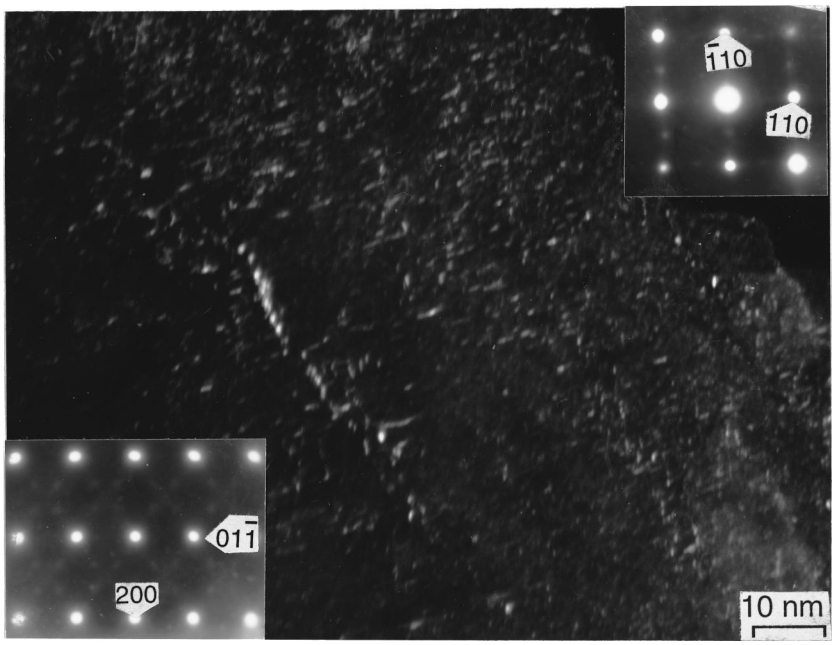

FIG. 8. Dark field (DF) micrograph, using 1/2 (110) reflections, showing the presence of ω-phase particles. The inset at the top shows the selective area diffraction (SAD) pattern of these reflections. The inset at the bottom is $\langle 110 \rangle$ SAD pattern from the bcc matrix. It shows reflections at 1/3 and 2/3 positions of $\langle 112 \rangle$-type vectors confirming the presence of ω phase.

dies down faster than that at 430 °C. These findings are particularly interesting since the formation of ω-related phases involves the collapse of the parent lattice by a displacement wave. It is conjectured that the collapse is preceded by chemical ordering making the process of ordered ω precipitation necessarily thermally activated. At the beginning of this precipitation process, the interface is more diffused but as the aging proceeds, the precipitate-matrix boundaries become sharper. It is noteworthy that the WAXS profiles, Fig. 7, from cold-rolled (CR) specimens have weak side peak.

A clear evidence of formation of ω phase is also obtained in the electron diffraction patterns. One typical pattern from a specimen aged at 430 °C for 25 h is shown in Fig. 8. The initial stages of the formation of characteristic ω phase are seen as diffused streaks in the diffraction patterns.

At temperatures above 450 °C, the nucleation of A_3B type of precipitates occurs through concentration fluctuations rather than through the collapse of the lattice. In this case, the conversion of an embryo into a nucleus through a concentration fluctuation results in sharp interfaces relatively quickly with well defined composition of the nucleus. The diffraction patterns therefore contain clear spots corresponding to phases like $Ni_3(Ti,Mo)$ as shown in Fig. 9. These studies hint at the existence of two distinct time-temperature-transformation (TTT) curves for precipitation in maraging steels, one below 450 °C and the other above this temperature. A schematic of time-temperature-transformation (TTT) curves illustrating this feature is shown in Fig. 10.

The SAXS scattering profiles, as depicted in Figs. 1, 2, and 3, have been analyzed in the light of interacting hard-sphere approximation.[31,32] The profiles are best interpreted in terms of radius dispersion $\rho(R)$ of the secondary phase in the form of Weibull distribution,

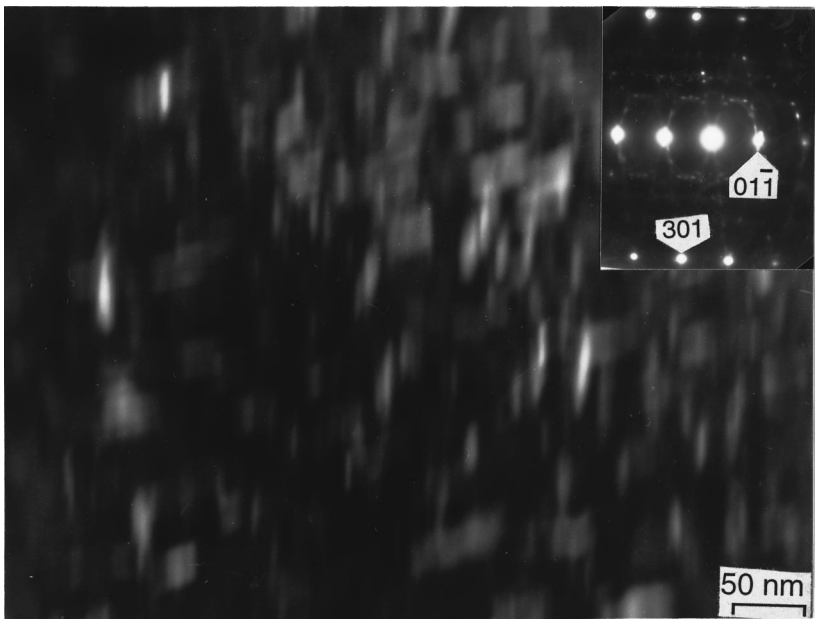

FIG. 9. Dark field (DF) micrograph of a specimen aged at 510 °C for 30 min. The inset shows the $\langle 113 \rangle$ zone of the bcc matrix. The additional spots could be indexed in terms of different variants of $Ni_3(Ti,Mo)$.

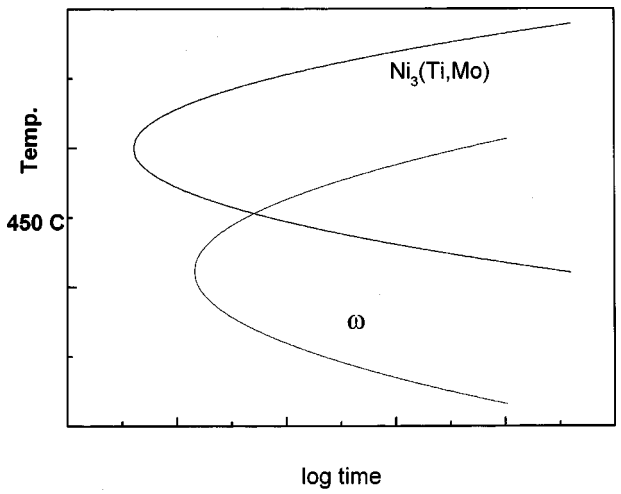

FIG. 10. A schematic of time-temperature-transformation (TTT) curve of 350-grade maraging steel.

$\rho(R)=c(R/R_0)^{b-1}\exp[-(R/R_0)^b]$, where c is the normalization constant and R_0 and b are adjustable parameters. The results of the fit are given in Table II where ϕ denotes the volume fraction of the precipitates and γ denotes the ratio of the two radii, corresponding to the hard sphere and the precipitate, respectively. R_1 and R_2 denote the first and second moment of the radius distribution, respectively. The variation of R_1 with time at 430 and 510 °C are shown in the insets of Figs. 1 and 2, respectively. R_1 follows a scaling law with aging time with exponent 0.2152, somewhat closer to 1/5, at 430 °C and with exponent 0.35, close to 1/3, at 510 °C.

In order to examine the scattering function kinetics in the light of scaling phenomena of unmixing in alloy system,[4,6,11–13,16] we have calculated the normalized scaling function $F(q/q_1(t))=[q_1(t)]^3S(q,t)/\Sigma q^2S(q,t)\delta q$ where $q_1(t)$ and δq are the first moment of the scattering function $S(q,t)$ and experimental q increment, respectively. The plots of $F(q/q_1(t))$ for specimens with different aging time at 430 and 510 °C are shown in Figs. 11, 12, and 13, respectively. From Fig. 11, it is evident that the scaling function $F(q/q_1(t))$ is independent of time[4,6] up to an aging time of 7 h. At this temperature, $F(q/q_1(t))$ scales as $(q/q_1)^{-4.43\pm0.19}$ for large (q/q_1). From Fig. 12 it is evident that time-independent feature of scaling function is observed up to 15 min at 510 °C. $F(q/q_1(t))$ scales as $(q/q_1)^{-4.21\pm0.16}$ for large (q/q_1) indicating diffused interfaces between precipitates and the matrix. Beyond these points, the change of the scaling function takes place in a rather broad time range at both the temperatures. Irrespective of aging temperature, phase separation broadly follows two distinct patterns. In the initial stage, dynamical scaling holds for the scattering function $S(q,t)$ which exhibits $q^{-(4+\delta)}$ (where $\delta>0$) for high q values. No q^{-2} law[3] was observed. However, at late stage dynamical scaling does not hold good but q^{-4} law holds. These observations are in sharp contrast with those obtained[10,17] with AlZn and FeCr alloys. In AlZn and FeCr alloys, at early stage dynamical scaling does not hold good for the scattering function $S(q,t)$ which exhibits q^{-2} power law for high q values as predicted by Langer, Bar-on, and

TABLE II. The results from the fit of the polydisperse hard sphere following Weibull distribution. The parameters are defined in the text.

Sample specification (aging temperature and time)	ϕ	γ	R_0 (nm)	b	R_1 (nm)	R_2 (nm^2)
Recrystallized (RC)	0.011±0.001	1.001±0.027	1.142±0.008	3.001±0.12	1.02±0.03	1.178±0.059
RC,430 °C and 30 min	0.012±0.001	1.016±0.027	1.697±0.012	3.2±0.128	1.52±0.05	2.582±0.129
RC,430 °C and 1.0 h	0.014±0.001	1.025±0.028	1.954±0.014	3.48±0.139	1.758±0.05	3.403±0.17
RC,430 °C and 3.0 h	0.016±0.001	1.131±0.029	2.468±0.018	4.01±0.16	2.238±0.067	5.401±0.27
RC,430 °C and 7.0 h	0.02±0.002	1.146±0.029	2.976±0.022	4.13±0.17	2.702±0.081	7.843±0.392
RC,430 °C and 18.0 h	0.041±0.004	1.201±0.032	3.556±0.026	5.31±0.21	3.279±0.098	11.257±0.563
RC,430 °C and 24 h	0.052±0.005	1.182±0.032	3.794±0.028	5.48±0.22	3.502±0.105	12.808±0.64
RC,430 °C and 48.5 h	0.074±0.007	1.176±0.032	4.383±0.032	5.889±0.24	4.062±0.122	17.141±0.857
RC,430 °C and 72.0 h	0.098±0.009	1.192±0.032	4.753±0.035	6.153±0.25	4.416±0.132	20.2±1.01
RC,510 °C and 5 min	0.026±0.002	1.023±0.028	2.284±0.017	4.7±0.19	2.09±0.062	4.624±0.232
RC,510 °C and 15 min	0.042±0.004	1.021±0.027	3.339±0.024	5.1±0.2	3.07±0.092	9.902±0.495
RC,510 °C and 30 min	0.075±0.007	1.036±0.028	4.264±0.031	4.95±0.2	3.913±0.117	16.13±0.806
RC,510 °C and 1.0 h	0.087±0.008	1.042±0.028	5.321±0.039	7.12±0.29	4.982±0.149	25.499±1.275
RC,510 °C and 3.0 h	0.096±0.009	1.066±0.03	7.684±0.056	9.52±0.38	7.295±0.219	54.062±2.71
RC,510 °C and 6.0 h	0.108±0.01	1.109±0.03	9.765±0.071	11.58±0.46	9.345±0.28	88.286±4.414
RC,510 °C and 18.0 h	0.12±0.011	1.202±0.032	14.084±0.103	15.898±0.64	13.625±0.409	186.75±9.34
Cold rolled (CR)	0.023±0.002	1.012±0.027	2.027±0.015	3.34±0.13	1.82±0.054	3.672±0.185
CR,430 °C and 7.0 h	0.096±0.009	1.09±0.029	11.838±0.086	14.564±0.58	11.421±0.343	131.362±6.57
CR,430 °C and 18.0 h	0.106±0.01	1.182±0.032	16.053±0.048	19.897±0.79	15.626±0.469	245.12±12.251
CR,510 °C and 1.0 h	0.116±0.01	1.153±0.031	6.068±0.044	6.849±0.27	5.67±0.17	33.093±1.655

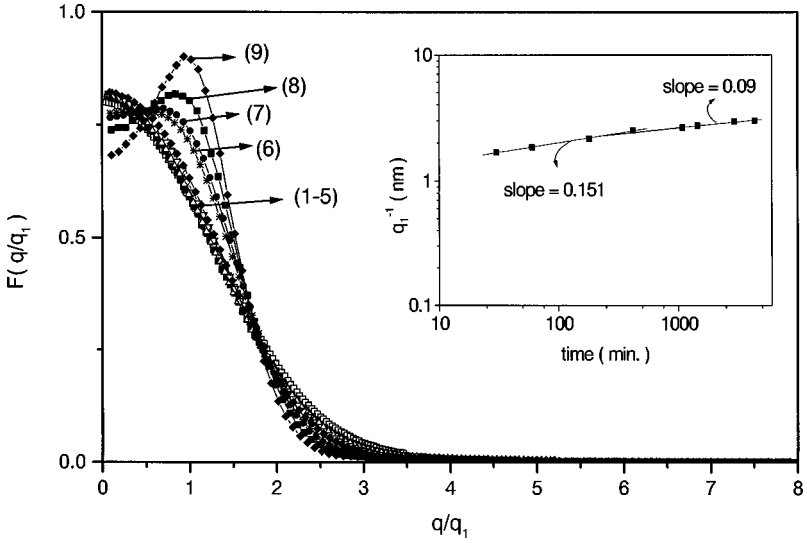

FIG. 11. Scaled scattering function $F(q/q_1)$ of 350-grade maraging steel aged at 430 °C for different durations of time. The correspondence of the profile number and the aging time is the same as mentioned in Fig. 1. The inset shows the variation of the reciprocal of $q_1(t)$ with time plotted on a logarithmic scale.

Miller.[3] At late stage, both q^{-4} law and dynamical scaling hold good. As discussed before, cold working a material introduces defect fields. Figure 13 indicates that the introduction of defect field is only detrimental to the scaling phenomena in the present material. It would be an interesting subject for future investigation to see if this phenomenon is valid for other materials too.

Since the cluster of the secondary phase can have any arbitrary shape, the consideration of growth of average cluster size with aging time is pertinent for the present investigation. The insets in Figs. 11 and 12 show the variation of the reciprocal of $q_1(t)$, proportional to average cluster size, with time. $q_1(t)$ follows a power law $t^{-\alpha}$. At 430 °C, there is a crossover of the scaling behavior of $q_1(t)$, i.e., the value of α is not uniform over the entire time range unlike the scaling behavior of R_1 shown in the insets of Figs. 1 and 2. At 430 °C, $\alpha = 0.15(\pm 0.01)$ up to 7 h and $\alpha = 0.09(\pm 0.004)$ beyond 7 h. At 510 °C, the value of α is uniform over the entire time range and is close to 1/4. These findings indicate the possibility of the nonunique characteristic length.

It is to be noted that the theory of Binder and Stauffer[2] predicted crossover phenomena where the value of α changes from 1/5 to 1/3 which is not in accord with the present observation. However, it is interesting to note that R_1, the first moment of the size distribution of secondary phase, follows a scaling law, shown by the inset in Fig. 1, with aging time with exponent close to 1/5 as predicted by the cluster dynamics of Binder and Stauffer.[2] Here the growth of the secondary phase is due to coalescence of clusters by a slow structural and compositional change in the material between them. This change is compatable with the structure and composition of clusters. At 510 °C, there is no crossover of the scaling behavior of $q_1(t)$ and $\alpha = 0.248(\pm 0.019)$ is uniform for the entire aging time range. R_1 follows a scaling law, shown by the inset in Fig. 2, with aging time with exponent close to 1/3 as theoretically predicted by the coarsening model of Lifshitz and Slyozov.[1] This coarsening model involves a condensation process in which clusters grow by the diffusion of single atoms one after the other from one stationary cluster to the other. It is noteworthy that at high temperature, viz. 510 °C, the growth is through diffusion of single atoms while at relatively lower temperature, viz. 430 °C, the growth is through diffusion of clusters. The size distributions of the precipitates are nar-

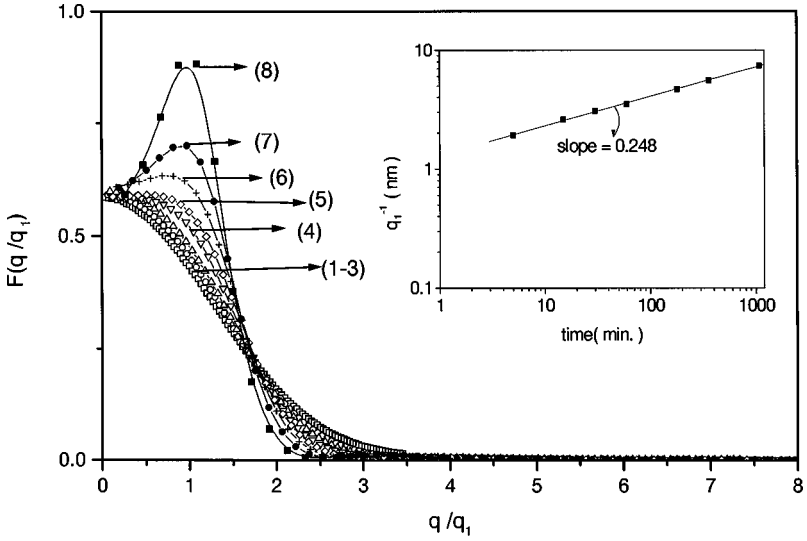

FIG. 12. Scaled scattering function $F(q/q_1)$ of 350-grade maraging steel aged at 510 °C for different durations of time. The correspondence of the profile number and the aging time is the same as mentioned in Fig. 2. The inset shows the variation of the reciprocal of $q_1(t)$ with time on a logarithmic scale.

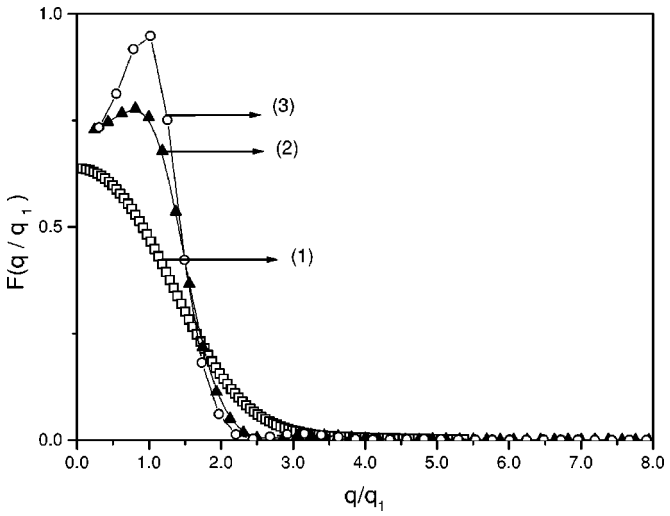

FIG. 13. Scaled scattering function $F(q/q_1)$ of cold-worked 350-grade maraging steel aged at 430 °C for different durations of time as mentioned below. (1) cold rolled (CR); (2) CR, 430 °C and 7.0 h; (3) CR, 430 °C and 18.0 h.

rowed down, indicated by the estimated b values listed in Table II, with increase in aging time for both the temperatures.

It is known that a cold-worked material gives pseudo-[33–35] small-angle scattering arising due to double-Bragg reflections. After annealing the specimens, we have investigated four cold-worked specimens with different aging treatments, namely, (1) no further aging, (2) 510 °C for 1 h, (3) 430 °C for 7 h and (4) 430 °C for 18 h. The distinct observations from the specimens aged in the cold-worked condition vis-à-vis similarly aged specimens without cold work are the following: The size distribution of the precipitates are shifted towards higher size as if cold work facilitates the growth of the precipitates. The distributions are narrower indicating more well defined precipitate size, and spatial correlation is significantly stronger indicating strong positional correlation of the precipitates enforced by the cold work. It appears that the mechanical process of cold rolling is providing, at least partially, the activation energy required for the precipitation phenomena. The above observations are in accord with the TEM investigation[36] of Ti-Nb alloy indicating strong positional correlation of ω particles because of the development of the texture due to cold work and faster growth kinetics brought about by increased dislocation density induced by cold work.

IV. CONCLUSION

From the present investigations, we conclude that the nature of the final precipitates and the routes through which these transformations occur appear to be different at the two temperatures. It could be due to different thermodynamic stability criterion at the two temperatures. From SAXS results, it is evident that kinetics of phase separation is different at the two specified temperatures. The system exhibits scaling phenomena but only at the early stage of phase separation. At the late stage, the scaling phenomenon does not hold good. Possibility exists for nonunique characteristic length. Average radius of the second phase follows different power laws at the two temperatures. There is no crossover phenomenon as far as the time scaling of the average radius is concerned, unlike the reciprocal of the first moment of q—which shows a different time scaling. Porod exponent being close to 5 is not indicative of the existence of multicomponent order parameter. TEM investigations clearly indicate that at each aging temperature, system exhibits only one order parameter as separation of only one phase takes place. Present investigation also hints at the possibility of existence of a time window within which scaling phenomenon holds good. Previous experiments already confirm the existence of minimum time below which scaling phenomenon does not hold good. The possibility exists that in the present investigation, the aging times are beyond the left-hand boundary of the time window. Some more experimentation are to be carried out to investigate the validity of scaling phenomenon at the very late stages of phase separation and also to investigate the existence of the aforementioned time window. Of course, the extremum limits of the time window will depend upon the diffusion constants of the relevant atomic species in the matrix.

From TEM experiments with specimens aged at 430 °C, the phase separation is attributed to the formation of ω phase through an instability in the bcc matrix. At 510 °C, the phase separation is attributed to the formation of $Ni_3(Ti, Mo)$ (DO_{24} structure) through the process of nucleation and growth. The system appears to follow two different time-temperature-transformation curves. The present study will contribute significantly in understanding the phase evolution processes in maraging steels and in designing suitable thermomechanical treatments for improving its mechanical properties.

ACKNOWLEDGMENTS

The authors are grateful to Dr. S. K. Sikka, Solid State Physics Group, BARC and Dr. C. K. Gupta, Materials Group, BARC, for their encouragement and keen interest in this work. The authors are also grateful to Technical Physics Division of BARC for vacuum sealing of specimens for the aging treatments. The help rendered by Mr. R. K. Fotedar towards rolling the material is also thankfully acknowledged.

*Electronic address: smazu@apsara.barc.ernet.in

[1] I.M. Lifshiftz and V. Slyozov, J. Phys. Chem. Solids **19**, 35 (1961).

[2] K. Binder and D. Stauffer, Phys. Rev. Lett. **33**, 1006 (1974).

[3] S. Langer, M. Bar-on, and H.D. Miller, Phys. Rev. A **11**, 1417 (1975).

[4] J. Marro, J.L. Lebowitz, and M.H. Kalos, Phys. Rev. Lett. **43**, 282 (1979).

[5] M. Hennion, D. Ronzaud, and P. Guyot, Acta Metall. **30**, 599 (1982).

[6] J.L. Lebowitz, J. Marro, and M.H. Kalos, Acta Metall. **30**, 297 (1982).

[7] S. Komura, K. Osamura, H. Fujii, and T. Takeda, Phys. Rev. B **30**, 2944 (1984).
[8] S. Katano and M. Iizumi, Phys. Rev. Lett. **52**, 835 (1984).
[9] S. Komura, K. Osamura, H. Fujii, and T. Takeda, Phys. Rev. B **31**, 1278 (1985).
[10] M. Furusaka, Y. Ishikawa, and M. Mera, Phys. Rev. Lett. **54**, 2611 (1985).
[11] H. Toyoki, Phys. Rev. A **42**, 911 (1990).
[12] A.J. Bray and S. Puri, Phys. Rev. Lett. **67**, 2670 (1991).
[13] F. Liu and G.F. Mazenko, Phys. Rev. B **45**, 6989 (1992).
[14] A.P.Y. Wong, P. Wiltzius, and B. Yurke, Phys. Rev. Lett. **68**, 3583 (1992).
[15] A.P.Y. Wong, P. Wiltzius, R.G. Larson, and B. Yurke, Phys. Rev. E **47**, 2683 (1993).
[16] A.J. Bray, Adv. Phys. **43**, 357 (1994).
[17] J. Mainville, Y.S. Yang, K.R. Elder, M. Sutton, K.F. Ludwig, and G.B. Stephenson, Phys. Rev. Lett. **78**, 2787 (1997).
[18] S. Bastea and J.L. Lebowitz, Phys. Rev. Lett. **78**, 3499 (1997).
[19] S. Floreen, Metall. Rev. **13**, 115 (1968).
[20] R.F. Decker, R.B.G. Yeo, J.T. Eash, and C.G. Breber, Mater. Des. Eng. **55**, 106 (1962).
[21] V.K. Vasudevan, S.J. Kim, and C.M. Wayman, Metall. Trans. A **21**, 2655 (1990).
[22] U.K. Viswanathanan, G.K. Dey, and M.K. Asundi, Metall. Trans. A **24**, 2429 (1993).
[23] D.T. Peters and C.R. Cupp, Trans. Metall. Soc. AIME **236**, 1420 (1966).
[24] C. Servant, G. Maeder, and G. Cizeron, Metall. Trans. A **6**, 981 (1975).
[25] C. Servant, N. Bouzid, and O. Lyon, Philos. Mag. A **56**, 565 (1987).
[26] S. Banerjee, R. Tewari, and P. Mukhopadhyay, Prog. Mater. Sci. **42**, 109 (1997).
[27] S.K. Sikka, Y.K. Vohra, and R. Chidambaram, Prog. Mater. Sci. **27**, 245 (1982).
[28] H. Amenitsch, S. Bernstorff, M. Kriechbaum, D. Lombardo, H. Mio, M. Rappolt, and P. Lagner, J. Appl. Crystallogr. **30**, 872 (1997).
[29] To be published separately.
[30] K. Kranjic, J. Appl. Crystallogr. **7**, 211 (1974).
[31] N.W. Ashcroft and J. Lekner, Phys. Rev. **145**, 83 (1966).
[32] W.K. Bertram, J. Appl. Crystallogr. **29**, 682 (1996).
[33] A. Guinier, J. Appl. Phys. **30**, 601 (1959).
[34] R.H. Neynaber, W.G. Brammer, and W.W. Beeman, J. Appl. Phys. **30**, 656 (1959).
[35] H. Fricke and V. Gerold, J. Appl. Phys. **30**, 661 (1959).
[36] V.S. Raghunathan, S. Raju, and A.L.E. Terrance, in *Metastable Microstructures*, edited by D. Bannerjee and L.A. Jacobson (Oxford & IBH Publishing Co., New Delhi, 1993), p. 161.